


Entanglement-Assisted Absorption Spectroscopy by Hong-Ou-Mandel Interference

Yuanyuan Chen^{Ⓞ,*}, Qian Shen[Ⓞ], Song Luo, Long Zhang, Zhanghai Chen, and Lixiang Chen[†]
Department of Physics and Collaborative Innovation Center for Optoelectronic Semiconductors and Efficient Devices, Xiamen University, Xiamen 361005, China

 (Received 22 July 2021; revised 30 September 2021; accepted 6 December 2021; published 7 January 2022)

Absorption spectroscopy has long been hailed as an absolute necessity for detecting the properties of complex chemical and biological samples. While conventional spectroscopy using classical light is severely limited by shot noise and lacks robustness against experimental imperfections, quantum light offers an avenue to perform absorption spectroscopy with provable advantages in the technical operations and the measurement precision. Here, we present an experimental approach to implement entanglement-based absorption spectroscopy with the assistance of Hong-Ou-Mandel interference. Since the temporal interference fringe is determined by the spectrum pattern, a maximum-likelihood decision is sufficient for revealing the relevant quantum information about the absorptive properties of the test samples. These experimental results may significantly facilitate the use of quantum interferometric spectroscopy to practical applications, which may be particularly relevant for photon-sensitive biological and chemical samples.

DOI: [10.1103/PhysRevApplied.17.014010](https://doi.org/10.1103/PhysRevApplied.17.014010)

I. INTRODUCTION

Absorption spectroscopy is routinely used to characterize the optical properties of materials and of chemical and biological samples [1–4]. Typically, the absorption spectroscopy of a sample is obtained by comparing the spectrum and intensity of the incident light and those of the transmitted light after the interaction with the target sample. Notably, the exploitation of an optical frequency comb—that is, a broad spectrum composed of equidistant narrow lines—enables alternative approaches for spectroscopy over broad spectral bandwidths. Additionally, the performance of a variety of existing spectrometers can be dramatically enhanced by using this optical frequency comb [5–7]. However, even for state-of-the-art laser absorption spectroscopy, the measurement precision is theoretically limited by shot noise due to the fundamental Poisson distribution of the photon number in laser radiation [8,9]. In practice, the shot-noise limit can only be achieved when all other sources of noise—for example, noise arising from the probe itself, from an imperfect environment, and from optical effects on the samples—are completely eliminated. Thus, how to perform absorption spectroscopy with high precision even in the presence of detrimental noise is still a formidable challenge.

In recent decades, quantum sensing and metrology has aroused great interest in the applications of positioning, timing, and mostly prominently the Laser Interferometer Gravitational Wave Observatory [10–13]. In contrast to classical resources, quantum sensing harnesses non-classical resources to substantially achieve the quantum advantages in the robustness against practical nonidealities and the measurement precision and accuracy [14]. Wavelength-correlated and tunable photon pairs have been used to perform absorption spectroscopy with precision near the ultimate quantum limit, which indicates that single photons are the optimal probe for absorption measurement [15,16]. In a conventional scheme, single photons in a signal or idler path are directly interacted with absorptive samples. Then, at the output of the experimental setup, the photons from each path are coupled into multimode fibers and sent through to avalanche-photodiode single-photon detectors with coincidence logic. According to the reduced intensity with respect to the incident light without interaction with the test samples, it is possible to deduce the absorptive ratio of the samples at the wavelength of the signal or idler photons. As the excess noise and the thermal loss channel can influence the transmission ratio, this method is susceptible to experimental imperfection, with the result that the precision and resolution of this absorption spectroscopy scheme are significantly limited. There has been a broad consensus that single photons with narrower-frequency bandwidths enable us to obtain a higher spectral resolution. Nevertheless, the

*chenyy@xmu.edu.cn

†chenlx@xmu.edu.cn

generation of spectrally narrow photons would reduce the pair-generation rate, which inversely imposes the ultimate limit on the precision [17,18]. To tackle this issue, Shi *et al.* have proposed a well-designed theoretical system that exploits entanglement to probe the absorption spectra, where an optical parametric amplifier (OPA) is applied on the returned entangled photon pairs [19]. However, the complexity and efficiency aspects of the experimental implementation of OPA still face significant technological challenges.

Quantum interference of entangled photons has engendered tremendous intriguing phenomena that lack any counterpart in classical physics [20]. Hitherto, owing to the salient properties of quantum optics, quantum interference have been widely studied and provides useful tools for ultrasensitive quantum metrology [13,21]. Hong-Ou-Mandel (HOM) interference, the fact that identical photons that arrive simultaneously at different input ports of a beam splitter bunch into a common output port, is a prototypical example of such a quantum phenomenon [22]. Since the quantum interference fringes are directly related to the level of indistinguishability of the photon, the HOM interferometer has been widely used in applications of quantum metrology [23–25]; in particular, for those photon-sensitive biological and chemical samples [1,9,26]. This leads to a question of the utmost importance: Is it possible to implement absorption spectroscopy with the assistance of HOM interference? In other words, how can we construct a quantum interferometric spectrometer based on quantum interference patterns [27]?

Here, we embark on an alternative route toward robust and precise entanglement-based absorption spectroscopy. We use one of the entangled photons to interact with the target absorptive sample and exploit the HOM interference on the detection side. The resultant interference fringes observed by the twofold coincidences between two output ports of the HOM interferometer reveal the non-classical frequency beating signals. Then, we perform a maximum-likelihood decision on the measurement results to retrieve the absorptive spectra. Backed by the results of our proof-of-concept experiment, this shows that our approach can implement quantum interferometric spectroscopy. As a result of the inherent stability of the HOM interferometer even in the presence of fluctuations of path-length difference that are on the order of the wavelength, this approach has the potential to achieve the provable quantum advantages over the optimum classical systems.

Beyond its appeal for applications, our approach indicates the fundamental link between the spectral and temporal degrees of freedom of the biphoton wave function. Apart from the entanglement-based absorption spectroscopy presented in this work, this approach may also have potential applications in spectral-domain quantum optical coherence tomography, which can achieve great advantages in measurement resolution and capture time

[28]. Furthermore, we also believe that this connection can provide additional tools, e.g., interferometric three-dimensional tomography [29], ultimately broadening the path toward practical quantum information processing and quantum interferometric metrology.

II. THEORETICAL SCHEME

Let us now consider an experimental configuration as shown in Fig. 1. A diode laser pumps the nonlinear optical crystals, phase-matched for collinear type-0 spontaneous parametric down-conversion (SPDC). A half-wave plate (HWP) in the pump beam is used to set a diagonal polarization state, such that two mutually orthogonally oriented nonlinear crystals are pumped equally. This generates pairs of parallel-polarized photons $|HH\rangle$ in the first crystal and $|VV\rangle$ in the second crystal in the identical spatial mode [17,30]. Rotating the polarization of the down-converted photons to the diagonal and antidiagonal directions and setting the relative phase $\phi = \pi$, the resultant state reads as follows:

$$(|AA\rangle - |DD\rangle)/\sqrt{2} = (|HV\rangle + |VH\rangle)/\sqrt{2}. \quad (1)$$

Subsequently, the photons within a pair are deterministically separated into two distinct spatial modes by using a polarizing beam splitter (PBS). The photon pairs are generated in a low-gain-parameter regime of SPDC and so are modeled as color entanglement:

$$|\Psi\rangle = \sum_{mn} A_{mn}(\omega_m\omega_n + \omega_n\omega_m), \quad (2)$$

where the correlated frequencies satisfy the energy-conservation principle as $\omega_m + \omega_n = \omega_p$ and A_{mn} denotes the probability amplitude for each pair of frequency-bin entanglement in a two-dimensional subspace.

The signal photons then pass through a translation stage, which can be tuned to introduce a relative time delay τ . As an absorptive sample is placed in the idler path, the idler photons interact with this target absorptive sample and this results in a scraggly spectral distribution. Correspondingly, the joint spectral intensity of the biphoton wave function is changed, followed by the transformation of the frequency-bin entanglement as

$$|\Psi\rangle \rightarrow \sum_{mn} A_{mn}(X_m\omega_m\omega_n + X_n\omega_n\omega_m), \quad (3)$$

where X_m and X_n are target parameters for absorption spectroscopy. These pairs of photons are incident on a balanced beam splitter from opposite input ports, which constitutes a HOM interferometer. The time delay between the time of arrival of the photons on the balanced beam splitter

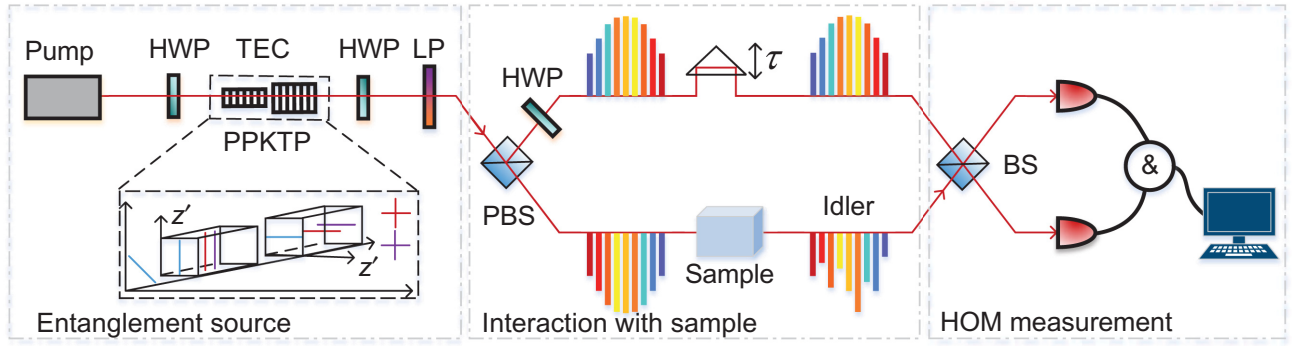


FIG. 1. A diagram of absorption spectroscopy assisted by Hong-Ou-Mandel interference: HWP, half-wave plate; TEC, temperature controller; PPKTP, periodically poled potassium titanyl phosphate crystal; LP, long-pass filter; PBS, polarizing beam splitter; BS, balanced beam splitter; $D_{1/2}$, single-photon detector; &, electronic AND gate. The inset in the entanglement source part illustrates the horizontally and vertically orientated crystals, which ensure that the incident diagonally polarized photons can pump these two crystals with equal probability.

would introduce a wavelength-dependent phase shift in the entangled state as follows:

$$|\Psi\rangle \rightarrow \sum_{mn} A_{mn} (X_m \omega_m \omega_n + e^{i\Delta\omega_{mn}\tau} X_n \omega_n \omega_m), \quad (4)$$

where $\Delta\omega_{mn} = |\omega_m - \omega_n|$ is the frequency detuning of two well-separated frequency-entangled bins.

The nonclassical frequency beating can be identified by scanning the arrival times of the signal photons and the corresponding interference fringes can be observed in the twofold coincidences between the two output ports of the beam splitter. It has been presented in our recent work [31] that the interference pattern can be interpreted as the combination of the spatial beatings resulting from the coherent superposition of multiple pairs of frequency-bin-entangled photons. In analogy to interference probability for two-dimensional frequency entanglement [32], we can rewrite

$$P(\tau) = \sum_{mn} \frac{A_{mn}}{4} \left[X_m^2 + X_n^2 + 2 \min(X_m^2, X_n^2) \cos(\Delta\omega_{mn}\tau + \varphi) \left(1 - \left| \frac{2\tau}{\tau_c} \right| \right) \right], \quad (5)$$

where τ_c is the single-photon coherence time, which equals the base-to-base envelope width, and φ is a phase offset. This indicates that discrete frequency entanglement manifests itself in sinusoidal oscillations of the interference fringes within a Gaussian envelope as a function of the relative time delay. Since the oscillation period in the interference pattern is determined by the frequency detuning $\Delta\omega_{mn}$, we can obtain the estimators of the probability amplitude parameters X_m and X_n by directly using nonlinear curve fitting. For an instructive means of understanding, this approach can be considered as a quantum

version of spectrum analysis, which decomposes the complex periodic vibration into a series of simple harmonic motions as shown in Fig. 2.

However, the single measurement of a HOM interference fringe can only offer two values, A_1 and A_2 ($A_1 < A_2$), for X_m or X_n but cannot indicate which value is for X_m and which is for X_n . To tackle this issue, we need a reference sample, the spectral absorptive factors Y_m and Y_n of which are already known. We place this known sample into the idler path and scan the arrival time of the signal photons again to obtain a second interference fringe. By the same token, we are allowed to obtain two values B_1 and B_2 ($B_1 < B_2$) for $X_m Y_m$ and $X_n Y_n$. In the scenario of $Y_m < Y_n$, if $B_1/B_2 < A_1/A_2$, then $X_m = A_1$ and $X_n = A_2$, while if $B_1/B_2 > A_1/A_2$, then $X_m = A_2$, and $X_n = A_1$. Conversely, in the scenario of $Y_m > Y_n$, if $B_1/B_2 < A_1/A_2$, then $X_m = A_2$ and $X_n = A_1$, while if $B_1/B_2 > A_1/A_2$, then $X_m = A_1$ and $X_n = A_2$.

While a Fourier transform on the HOM interference fringe may also reveal the spectral pattern [27], maximum-likelihood estimation (MLE) based on nonlinear curve fitting enables us to adaptively modulate the statistical model based on the practical experimental setup. This would further enhance the measurement precision of our method even in the presence of detrimental experimental imperfections. The MLE procedure used in this work is analogous to robust high-dimensional quantum state tomography [33,34]. Specifically, in each iteration, our algorithm predicts the HOM interference pattern as shown in Eq. (5) by taking a random quantum state $|\sigma\rangle$ as the input and measures the overlap between its theoretical simulation and the experimental results. Starting from a current estimate $|\sigma_k\rangle$, we use a self-guided tomography that chooses one random direction and update the estimate state as $|\Psi\rangle = |\sigma_k + \beta_k\rangle$, where $|\beta_k\rangle$ represents the length of each step. After all iterations, we select the estimated state that has the maximum overlap between its theoretically

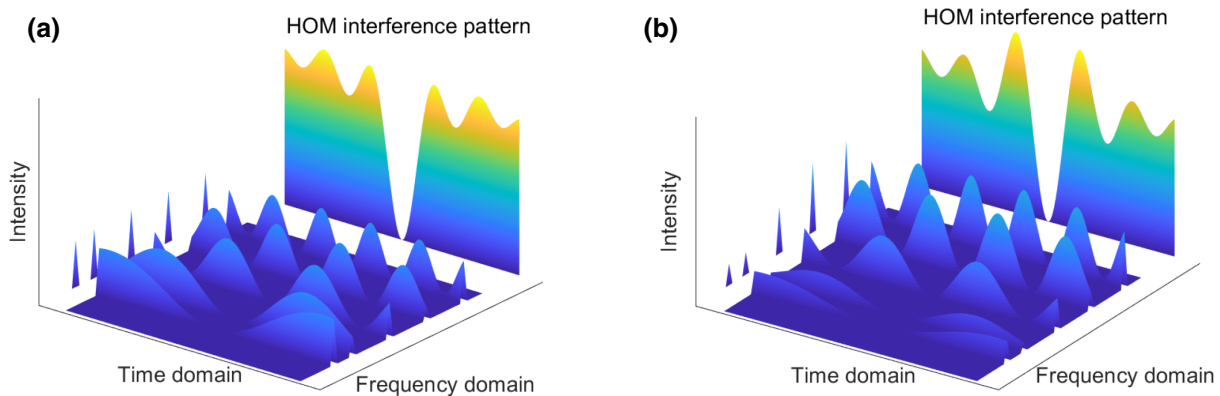


FIG. 2. Spectral analysis can decompose the HOM interference fringes into a series of simple quantum beat notes of two-dimensional frequency-bin entanglement with various frequency detunings. A theoretical simulation of HOM interference that is parametrized by five frequency detunings with (a) equal and (b) unequal probability amplitudes.

simulated interference pattern and the experimentally measured results. This method enables us to find the optimal estimator in the whole Hilbert space, even in the presence of detrimental noise. In contrast to direct Fourier transform, this MLE allows us to take experimental nonideality into the analysis of a statistical module, the target of which, in brief, is to search for the optimal estimator rather than the direct observation. Consequently, this MLE also offers great advantages in our absorption spectroscopy, as it has already achieved in the performance of phase measurement and state tomography [33–36].

III. EXPERIMENTAL IMPLEMENTATION

In our experimental realization (see Fig. 1), a pair of 5-mm-long type-0 periodically poled potassium titanyl phosphate (PPKTP) crystals are placed along the horizontal and vertical directions and pumped with a 405-nm continuous-wave grating-stabilized laser diode. They provide type-0 collinear phase matching with the pump (p), signal (s), and idler (i) photons at center wavelengths of $\lambda_p \approx 405$ nm and $\lambda_{s,i} \approx 810$ nm at a temperature of 21 °C. By superimposing the down-converted photons emitted from both crystals according to Eq. (1), they are sorted into distinct spatial modes deterministically by using a PBS. Since leaked pump photons would degrade the precision of our estimator and could lead to overexposure of the sample from unwanted wavelengths, the residual pump light is filtered out by using a long-pass filter. We also verify that these optics enable us to remove the pump photons through a single-photon-sensitive spectrometer. A HWP is placed in the signal path to eliminate the polarization distinguishability and a band-pass filter is utilized to adjust the spectral bandwidth of the generated entangled state. To explore the nonclassical beating of frequency entanglement in HOM interference, spatial interference can be observed by scanning the time of arrival of the photons that are incident

on the balanced beam splitter. Finally, the down-converted photons are detected by silicon avalanche-photon diodes and twofold events are identified using a fast electronic AND gate when two photons arrive at the detectors within a coincidence window of approximately 1 ns.

In a proof-of-principle experiment, we begin with experimental reconstruction of the absorption spectroscopy of two optical microcavities, the resonance wavelengths of which are at 806 nm and 810 nm, respectively. The microcavities consist of a half-wavelength cavity layer (SiO_2) sandwiched by two distributed Bragg reflectors (DBRs; six pairs of $\text{SiO}_2/\text{Si}_3\text{N}_4$). We place these two target samples in the idler path such that they can interact with the idler photons. The observed HOM interference patterns with subtraction of accidental coincidences versus the arrival time of the signal photons are shown in Figs. 3(a)–3(c), where the interference fringes of the subentanglement extracted by fitting the experimental data to Eq. (5) are also described. Specifically, as the frequency bandwidth of the initial down-converted photons is approximately 34 nm, these spectra are sampled by averaging them within each of $m = 13$ frequency bins. According to strict energy conservation, as a direct result of the exploitation of the pump with an ultranarrow frequency line width, the target parameters to be estimated are the probability amplitudes of seven pairs of subentanglement with frequency detunings $\mu = 0$ THz, $\mu = 3.2$ THz, $\mu = 6.5$ THz, $\mu = 9.7$ THz, $\mu = 12.9$ THz, $\mu = 16.2$ THz, and $\mu = 19.4$ THz. By following the MLE as presented in Sec. II, we calculate the overlap between the theoretically simulated interference pattern from Eq. (5) and the experimentally measured results and choose the quantum state that has the maximal overlap as the optimal estimator. Thus, curve fitting of the experimental results to Eq. (5) reveals the corresponding parameters in the high-dimensional state space, enabling us to obtain the probability amplitudes that are directly related to the absorption spectroscopy. Figures 3(d)–3(f)

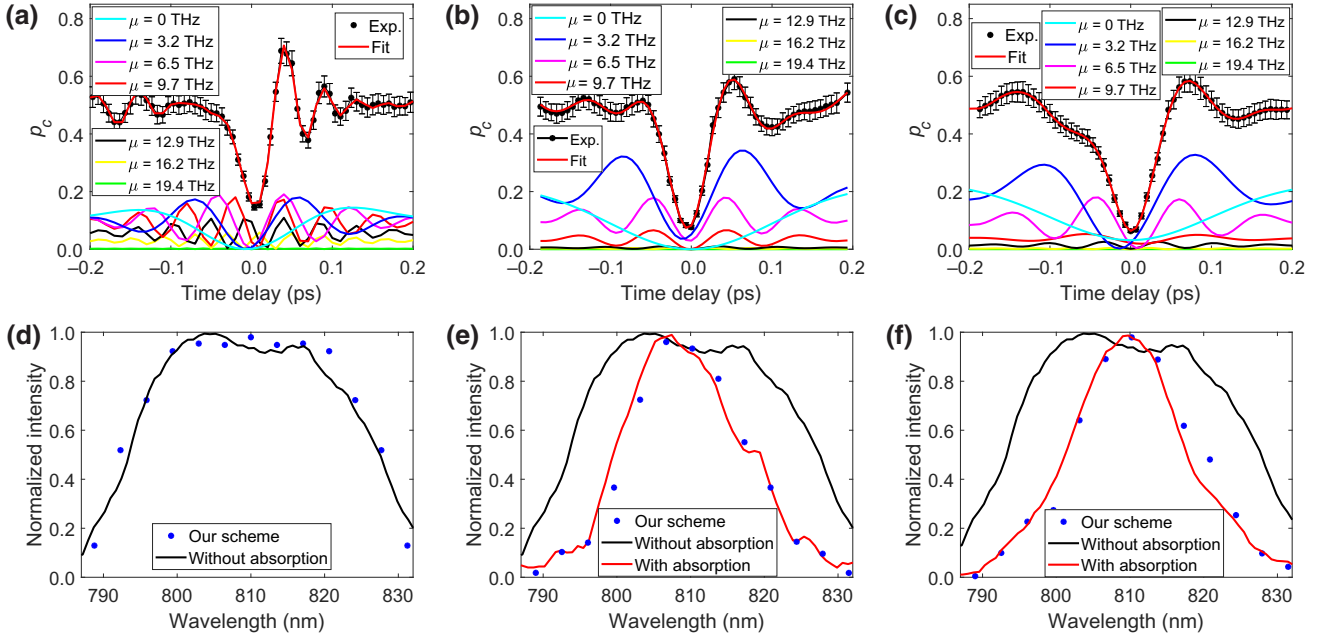


FIG. 3. Experimental results of absorption spectroscopy with the assistance of HOM interference. The experimentally observed HOM interference patterns (a) without an absorptive sample and (b),(c) with absorptive samples at a resonance wavelength of (b) 806 nm and (c) 810 nm (see the black dots), where the red lines represent the fitting curves. The error bars represent the standard deviation of the experimental results estimated by statistical methods assuming a Poisson distribution. The colored lines represent the interference patterns of subentanglement with various frequency detunings. Since the whole spectra are sampled by averaging them within each of $m = 13$ frequency bins and they satisfy strict energy conservation as a direct result of the exploitation of a pump with an ultranarrow frequency line width, seven pairs of subentanglement result, with frequency detunings $\mu = 0$ THz, $\mu = 3.2$ THz, $\mu = 6.5$ THz, $\mu = 9.7$ THz, $\mu = 12.9$ THz, $\mu = 16.2$ THz, and $\mu = 19.4$ THz. (d)–(f) The construction of the spectral distribution (d) before the interaction with the absorptive sample and after the interaction with absorptive samples at resonance wavelengths of (e) 806 nm and (f) 810 nm, where the black and red lines are experimental results observed by a single-photon spectrometer and the estimation results are shown by blue data points.

show the reconstructed spectroscopy of single photons after the interaction with absorptive samples (blue dots) and the real spectral distributions observed by the single-photon spectrometer are also demonstrated (black and red lines). The experimental results obtained by using our scheme agree well with the observations by using a single-photon spectrometer, where slight deviations can be attributed to imperfect experimental components and data analysis.

Notably, as opposed to direct intensity measurement based on a single-photon spectrometer or other interferometric approaches based on first-order interference, HOM interference is unaffected by variations in the optical phase. As a consequence, a HOM interferometer maintains its ability for precise metrology, even in the presence of fluctuations of path-length difference that are on the order of the wavelength. This feature has resulted in proposals for HOM-based sensors with an ultrahigh resolution [23] and protocols such as quantum optical coherence tomography that benefit from other quantum features such as the cancellation of some deleterious dispersion effect [24]. While this work confirms the viability of entanglement-assisted absorption spectroscopy by HOM

interference, the inherent nature of the HOM interferometer has the potential to provide great advantages in measurement resolution and precision.

IV. DISCUSSION

It has been shown in Ref. [19] that entanglement-assisted absorption spectroscopy achieves a provable quantum advantage in the discrimination of arbitrary absorption patterns over all spectroscopic schemes based on classical schemes. Likewise, we also consider two simplified problems: absorption detection and peak positioning. As proved in the earlier work, the error probability for absorption detection and the single-peak position of entanglement-assisted absorption spectroscopy is given by [19]

$$P_E = R_m \left[\frac{1}{1 + N_s(1 - \sqrt{\kappa_T})} \right]^{2M}, \quad (6)$$

where R_m is a random error probability when a zero count on the measurement operation occurs, N_s is the average mean photon number per frequency mode, κ_T

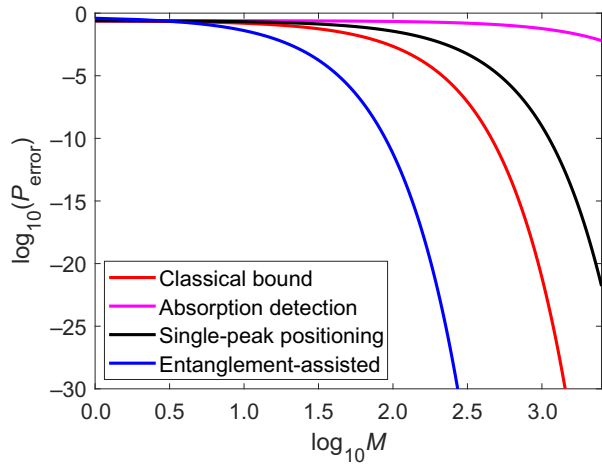


FIG. 4. The theoretical simulation of the error rate versus the number of experimental trials, with parameters $N_s = 1$ and $\kappa_T = 0.75$.

represents the transmissivity, and M is the number of independent trials needed to make a decision. The work reported in Ref. [19] claims that entanglement-assisted absorption spectroscopy has an exponential advantage of $\simeq 2 \exp[-MN_s(1 - \kappa_T)]$ for absorption detection and $\simeq 2 \exp[-2MN_s(\kappa_T - \sqrt{\kappa_T})]$ for single-peak positioning. Figure 4 demonstrates the error rates versus number of the probing modes with the practical parameters used in our experimental setup. In a classical spectroscopy scheme, the minimum error probability affecting the discrimination is inherently higher than the classical lower bound. In contrast, the error rate of absorption spectroscopy assisted by entanglement is obviously lower than the classical lower bound, which proves that entanglement-assisted absorption spectroscopy can offer an orders-of-magnitude advantage in error probability in the discrimination of sampled spectra even in the presence of experimental nonidealities.

Next, we consider a concise yet instructive application in the form of single-peak positioning. In a conventional absorption spectroscopy scheme, the absorption factors estimated from each single probe photon are distributed across the bandwidth of the photon—this is a limiting factor for both the resolution and precision of the measured spectra. If our scheme is applied to single-peak positioning, the achievable resolution would depend on the ultimate quantum limit of HOM interferometry. Once the distinguishability caused by frequency detuning is observable in the HOM interference pattern, we are able to deduce the specific absorptive spectra. Let us first recall the resolution of HOM interferometry on a biphoton beat note. In the case of a real HOM interferometer, which is subject to photon loss γ and imperfect experimental visibility α ,

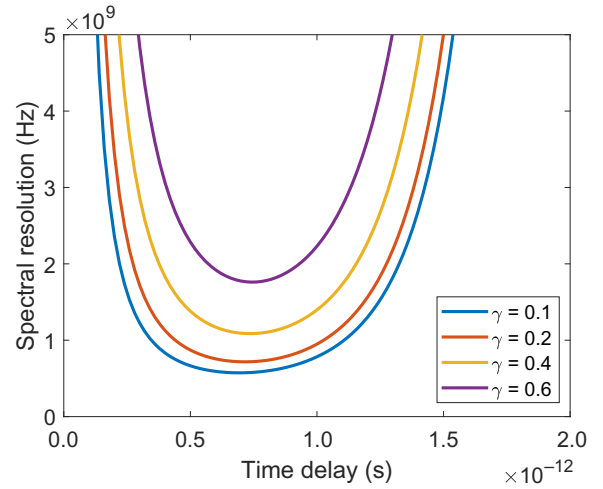


FIG. 5. The resolution limit of absorption spectroscopy in the scenarios of various photon loss rates. The coherence time $\tau_c = 1$ ps and the experimental trials $M = 10^5$.

the corresponding probability distributions read

$$\begin{aligned}
 P_2(\Delta\omega) &= \frac{1}{2}(1 - \gamma)^2 \left[1 + \alpha \cos(\Delta\omega\tau) e^{-2\sigma^2\tau^2} \right], \\
 P_1(\Delta\omega) &= \frac{1}{2}(1 - \gamma)^2 \left[\frac{1 + 3\gamma}{1 - \gamma} - \alpha \cos(\Delta\omega\tau) e^{-2\sigma^2\tau^2} \right], \\
 P_0(\Delta\omega) &= \gamma^2,
 \end{aligned} \tag{7}$$

where the subscripts 0, 1, and 2 denote the number of detectors that click, corresponding to total loss, bunching, and coincidence, respectively. For a more detailed discussion, see Ref. [23,25]. An estimator of $\Delta\omega$ is a function of the experimental data that allows us to infer the value of

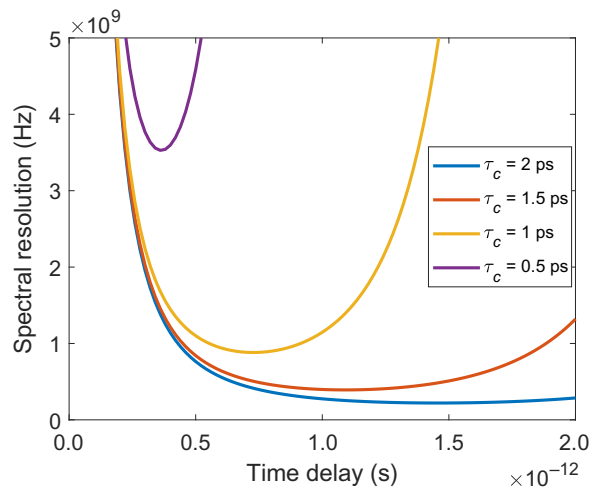


FIG. 6. The resolution limit of absorption spectroscopy in the scenarios of various coherence times. The photon loss rate is set to be $\gamma = 0.3$ and in the experimental trials, $M = 10^5$.

the unknown spectral positioning using a particular statistical model for the probability distribution of measurement outcomes. For any such estimator, the ultimate limit on the precision is known as the Cramér-Rao bound in the classical estimation theory, which states that the standard deviation is lower bounded by

$$\delta\omega_{CR} = \frac{1}{(MF_\omega)^{1/2}}, \quad (8)$$

where M is the number of independent experimental trials, and the Fisher information F_ω reads

$$F_\omega = \frac{[\partial_{\Delta\omega}P_2(\Delta\omega)]^2}{P_2(\Delta\omega)} + \frac{[\partial_{\Delta\omega}P_1(\Delta\omega)]^2}{P_1(\Delta\omega)} + \frac{[\partial_{\Delta\omega}P_0(\Delta\omega)]^2}{P_0(\Delta\omega)}. \quad (9)$$

Figure 5 shows the theoretically predicted resolution of absorption spectroscopy, wherein the resolution becomes lower with respect to an increase in the photon loss. As shown in Fig. 6, the resolution is enhanced as the single-photon coherence time is increased. For example, this method can provide an ultimate resolution of approximately 200 MHz for a coherence time of approximately 2 ps, a limit that satisfies the requirements of atomic spectroscopy. We note that the theoretical simulation is performed under the assumption of perfect measurement and analysis of the HOM interference fringes. We also note that the optimal probe is not at the position $\tau = 0$ in the presence of photon loss, which agrees well with the theoretical prediction of HOM interferometry.

V. CONCLUSION

We demonstrate an approach to the implementation of entanglement-based absorption spectroscopy with the assistance of HOM interference, which has the potential to provide advantages in the robustness against detrimental noise and the measurement precision and accuracy. This may be particularly relevant for photon-sensitive biological and chemical samples. Additionally, this work indicates a link between the spectral and temporal degrees of freedom of the biphoton wave function. We believe it can inspire more applications in quantum interferometric metrology, such as spectral-domain quantum optical coherence tomography [37].

Although the test samples used in our proof-of-principle experiment are relatively simple, the evaluation of these remarkable advantages of entanglement-assisted absorption spectroscopy is also very interesting, in particular for those complicated samples with hyperfine structures. In order to satisfy the specific requirements for these applications, the initial spectrum of down-converted photons should be sampled with a much narrower bandwidth and thus the resolution is further enhanced. By

following our method, it is possible to extract the individual probability amplitudes of frequency entanglement and reconstruct the absorption spectrum based on statistical analysis of the experimental results. However, it is still necessary to emphasize that the HOM interference pattern should be measured with a sufficiently small sampling step, which inversely affects the discrimination of the MLE algorithm. Besides, there are also several aspects of our scheme that can be improved for greater performance. (i) As demonstrated in Fig. 6, the generation of photons with narrow bandwidths (long coherence times) can further enhance the measurement precision, which is part of the inherent nature of interferometric metrology [23]. (ii) It is revealed in Eq. (8) that the measurement resolution is inversely proportional to the number of independent experimental trials [38]. Improvement of the efficiency of the overall experimental system—for example, by increasing the entangled-photon-pair generation rate by using longer nonlinear crystals or increasing the detection efficiency by replacing the avalanche photodiodes with number-resolving detection—can circumvent this limit on the photon pair-production rate. (iii) Hong-Ou-Mandel interferometry based on discrete frequency-entangled states with a large nondegeneracy has the potential to enhance the resolution and precision of measurement [25]. (iv) Increasing the accuracy of MLE by using optimal algorithms—for example, neural networks and deep learning—may enhance the performance of this absorption spectroscopy [39].

ACKNOWLEDGMENTS

This work is supported by the National Natural Science Foundation of China (NSFC) (Grants No. 12034016, No. 12004318, and No. 61975169), the Fundamental Research Funds for the Central Universities at Xiamen University (Grants No. 20720190057 and No. 20720200074), the Natural Science Foundation of Fujian Province of China (Grant No. 2020J05004), the Natural Science Foundation of Fujian Province of China for Distinguished Young Scientists (Grant No. 2015J06002), and the Program for New Century Excellent Talents in University, China (Grant No. NCET-13-0495).

-
- [1] M. A. Taylor and W. P. Bowen, Quantum metrology and its application in biology, *Phys. Rep.* **615**, 1 (2016).
 - [2] A. J. Tom Van Loon, *Analytical Atomic Absorption Spectroscopy: Selected Methods* (Elsevier, Amsterdam, Netherlands, 2012).
 - [3] J.-J. Velasco-Velez, C. H. Wu, T. A. Pascal, L. F. Wan, J. Guo, D. Prendergast, and M. Salmeron, The structure of interfacial water on gold electrodes studied by x-ray absorption spectroscopy, *Science* **346**, 831 (2014).

- [4] N. De Oliveira, M. Roudjane, D. Joyeux, D. Phalippou, J.-C. Rodier, and L. Nahon, High-resolution broadband Fourier-transform absorption spectroscopy in the VUV range down to 40 nm, *Nat. Photonics* **5**, 149 (2011).
- [5] N. Picqué and T. W. Hänsch, Frequency comb spectroscopy, *Nat. Photonics* **13**, 146 (2019).
- [6] L. C. Sinclair, K. C. Cossel, T. Coffey, J. Ye, and E. A. Cornell, Frequency Comb Velocity-Modulation Spectroscopy, *Phys. Rev. Lett.* **107**, 093002 (2011).
- [7] A. Foltynowicz, T. Ban, P. Masłowski, F. Adler, and J. Ye, Quantum-Noise-Limited Optical Frequency Comb Spectroscopy, *Phys. Rev. Lett.* **107**, 233002 (2011).
- [8] F. Wolfgramm, C. Vitelli, F. A. Beduini, N. Godbout, and M. W. Mitchell, Entanglement-enhanced probing of a delicate material system, *Nat. Photonics* **7**, 28 (2013).
- [9] M. A. Taylor, J. Janousek, V. Daria, J. Knittel, B. Hage, H.-A. Bachor, and W. P. Bowen, Biological measurement beyond the quantum limit, *Nat. Photonics* **7**, 229 (2013).
- [10] S. Pirandola, B. R. Bardhan, T. Gehring, C. Weedbrook, and S. Lloyd, Advances in photonic quantum sensing, *Nat. Photonics* **12**, 724 (2018).
- [11] I. R. Berchera and I. P. Degiovanni, Quantum imaging with sub-Poissonian light: Challenges and perspectives in optical metrology, *Metrologia* **56**, 024001 (2019).
- [12] C. L. Degen, F. Reinhard, and P. Cappellaro, Quantum sensing, *Rev. Mod. Phys.* **89**, 035002 (2017).
- [13] V. Giovannetti, S. Lloyd, and L. Maccone, Advances in quantum metrology, *Nat. Photonics* **5**, 222 (2011).
- [14] B. M. Escher, R. L. de Matos Filho, and L. Davidovich, General framework for estimating the ultimate precision limit in noisy quantum-enhanced metrology, *Nat. Phys.* **7**, 406 (2011).
- [15] R. Whittaker, C. Erven, A. Neville, M. Berry, J. L. O'Brien, H. Cable, and J. C. F. Matthews, Absorption spectroscopy at the ultimate quantum limit from single-photon states, *New J. Phys.* **19**, 023013 (2017).
- [16] G. Brida, M. Genovese, and I. R. Berchera, Experimental realization of sub-shot-noise quantum imaging, *Nat. Photonics* **4**, 227 (2010).
- [17] Y. Chen, S. Ecker, S. Wengerowsky, L. Bulla, S. K. Joshi, F. Steinlechner, and R. Ursin, Polarization Entanglement by Time-Reversed Hong-Ou-Mandel Interference, *Phys. Rev. Lett.* **121**, 200502 (2018).
- [18] S. Wengerowsky, S. K. Joshi, F. Steinlechner, H. Hübel, and R. Ursin, An entanglement-based wavelength-multiplexed quantum communication network, *Nature* **564**, 225 (2018).
- [19] H. Shi, Z. Zhang, S. Pirandola, and Q. Zhuang, Entanglement-Assisted Absorption Spectroscopy, *Phys. Rev. Lett.* **125**, 180502 (2020).
- [20] J.-W. Pan, Z.-B. Chen, C.-Y. Lu, H. Weinfurter, A. Zeilinger, and M. Żukowski, Multiphoton entanglement and interferometry, *Rev. Mod. Phys.* **84**, 777 (2012).
- [21] Z.-E. Su, Y. Li, P. P. Rohde, H.-L. Huang, X.-L. Wang, L. Li, N.-L. Liu, J. P. Dowling, C.-Y. Lu, and J.-W. Pan, Multiphoton Interference in Quantum Fourier Transform Circuits and Applications to Quantum Metrology, *Phys. Rev. Lett.* **119**, 080502 (2017).
- [22] C. K. Hong, Z. Y. Ou, and L. Mandel, Measurement of Subpicosecond Time Intervals between Two Photons by Interference, *Phys. Rev. Lett.* **59**, 2044 (1987).
- [23] A. Lyons, G. C. Knee, E. Bolduc, T. Roger, J. Leach, E. M. Gauger, and D. Faccio, Attosecond-resolution Hong-Ou-Mandel interferometry, *Sci. Adv.* **4**, eaap9416 (2018).
- [24] M. B. Nasr, B. E. A. Saleh, A. V. Sergienko, and M. C. Teich, Demonstration of Dispersion-Canceled Quantum-Optical Coherence Tomography, *Phys. Rev. Lett.* **91**, 083601 (2003).
- [25] Y. Chen, M. Fink, F. Steinlechner, J. P. Torres, and R. Ursin, Hong-Ou-Mandel interferometry on a biphoton beat note, *npj Quantum Inf.* **5**, 1 (2019).
- [26] K. M. Vitalis and I. K. Kominis, Quantum-limited biochemical magnetometers designed using the Fisher information and quantum reaction control, *Phys. Rev. A* **95**, 032129 (2017).
- [27] R.-B. Jin and R. Shimizu, Extended Wiener-Khinchin theorem for quantum spectral analysis, *Optica* **5**, 93 (2018).
- [28] P. J. Marchand, J. Riemensberger, J. C. Skehan, J.-J. Ho, M. H. P. Pfeiffer, J. Liu, C. Hauger, T. Lasser, and T. J. Kippenberg, Soliton microcomb based spectral domain optical coherence tomography, *Nat. Commun.* **12**, 1 (2021).
- [29] F. Devaux, A. Mosset, P.-A. Moreau, and E. Lantz, Imaging Spatiotemporal Hong-Ou-Mandel Interference of Biphoton States of Extremely High Schmidt Number, *Phys. Rev. X* **10**, 031031 (2020).
- [30] Y. Chen, S. Ecker, J. Bavaresco, T. Scheidl, L. Chen, F. Steinlechner, M. Huber, and R. Ursin, Verification of high-dimensional entanglement generated in quantum interference, *Phys. Rev. A* **101**, 032302 (2020).
- [31] Y. Chen, S. Ecker, L. Chen, F. Steinlechner, M. Huber, and R. Ursin, Temporal distinguishability in Hong-Ou-Mandel interference for harnessing high-dimensional frequency entanglement, *npj Quantum Inf.* **7**, 1 (2021).
- [32] Z. Y. Ou and L. Mandel, Observation of Spatial Quantum Beating with Separated Photodetectors, *Phys. Rev. Lett.* **61**, 54 (1988).
- [33] M. Rambach, M. Qaryan, M. Kewming, C. Ferrie, A. G. White, and J. Romero, Robust and Efficient High-Dimensional Quantum State Tomography, *Phys. Rev. Lett.* **126**, 100402 (2021).
- [34] A. Lumino, E. Polino, A. S. Rab, G. Milani, N. Spagnolo, N. Wiebe, and F. Sciarrino, Experimental Phase Estimation Enhanced by Machine Learning, *Phys. Rev. Appl.* **10**, 044033 (2018).
- [35] A. Hentschel and B. C. Sanders, Machine Learning for Precise Quantum Measurement, *Phys. Rev. Lett.* **104**, 063603 (2010).
- [36] M. Agnew, J. Leach, M. McLaren, F. S. Roux, and R. W. Boyd, Tomography of the quantum state of photons entangled in high dimensions, *Phys. Rev. A* **84**, 062101 (2011).
- [37] P. Yepiz-Graciano, A. M. A. Martínez, D. Lopez-Mago, H. Cruz-Ramirez, and A. B. U'Ren, Spectrally resolved Hong-Ou-Mandel interferometry for quantum-optical coherence tomography, *Photon Res.* **8**, 1023 (2020).
- [38] P. Kok and B. W. Lovett, *Introduction to Optical Quantum Information Processing* (Cambridge University Press, Cambridge, UK, 2010).
- [39] J. Biamonte, P. Wittek, N. Pancotti, P. Rebentrost, N. Wiebe, and S. Lloyd, Quantum machine learning, *Nature* **549**, 195 (2017).